SAND99-2779J

RECEIVED
NOV 02 1999
OSTI

# Density Functional Theory of Simple Polymers in a Slit Pore: 2. The Role of Compressibility and Field Type

Justin B. Hooper, Morgan T. Pileggi, John D. McCoy

Department of Materials & Metallurgical Engineering

New Mexico Institute for Mining & Technology

Socorro, New Mexico 87801

and

John G. Curro, Jeffrey D. Weinhold

Sandia National Laboratories†

Albuquerque, New Mexico 87185

†Sandia is a multiprogram laboratory operated by Sandia Corporation, a Lockheed Martin Company, for the U. S. Department of Energy under Contract DE-AC04-94AL85000.

**Abstract**

Simple tangent, hard site chains near a hard wall are modeled with a Density Functional (DF) theory that uses the direct correlation function, c(r), as its "input". Two aspects of this DF theory are focused upon: 1) the consequences of variations in c(r)'s detailed form; and 2) the correct way to introduce c(r) into the DF formalism. The most important aspect of c(r) is found to be its integrated value, $\hat{c}(0)$. Indeed, it appears that, for fixed $\hat{c}(0)$, all reasonable guesses of the detailed shape of c(r) result in surprisingly similar density distributions, $\rho(r)$. Of course, the more accurate the c(r), the better the $\rho(r)$. As long as the length scale introduced by c(r) is roughly the hard site diameter and as long as the solution remains liquid-like, the $\rho(r)$ is found to be in good agreement with simulation results.

The c(r) is used in DF theory to calculate the medium-induced-potential, $U_M(r)$ from the density distribution, $\rho(r)$. The form of $U_M(r)$ can be chosen to be one of a number of different forms. It is found that the forms for $U_M(r)$, which yield the most accurate results for the wall problem, are also those which were suggested as accurate in previous, related studies.

## DISCLAIMER

This report was prepared as an account of work sponsored by an agency of the United States Government. Neither the United States Government nor any agency thereof, nor any of their employees, make any warranty, express or implied, or assumes any legal liability or responsibility for the accuracy, completeness, or usefulness of any information, apparatus, product, or process disclosed, or represents that its use would not infringe privately owned rights. Reference herein to any specific commercial product, process, or service by trade name, trademark, manufacturer, or otherwise does not necessarily constitute or imply its endorsement, recommendation, or favoring by the United States Government or any agency thereof. The views and opinions of authors expressed herein do not necessarily state or reflect those of the United States Government or any agency thereof.

DISCLAIMER

Portions of this document may be illegible in electronic image products. Images are produced from the best available original document.

## 1. Introduction

The properties of polymers near solid surfaces are of obvious technological importance, and theories have been proposed for various surface properties. The current study has been directed towards a more complete understanding of the equilibrium structure and thermodynamics of inhomogeneous systems with the intent of eventually investigating wetting and adhesion issues; however, numerous other applications in both traditional and non-traditional polymers can be imagined.

Density functional (DF) theory was the methodology adopted for this study. In the previous paper[1], referred to here as Paper I, we reviewed the basic DF theory and described a new and highly efficient solution methodology while, in the current paper, DF theory is investigated with more accurate input and different medium induced potential types.

Density functional theory has evolved out of tools developed for the study of bulk liquid state properties. As a result, great emphases is placed upon the interaction-site correlation functions, with the inhomogeneous density, $\rho(r)$, being viewed as the analog of the pair correlation, $g(r)$, in bulk liquids. This analogy, however, should not be considered an equivalency.

The repulsive interactions, which are central to the understanding of the bulk liquid state, are also important to the complete understanding of surface properties such as adhesion. However, it should be appreciated that $\rho(r)$ is more strongly affected by the attractive contribution to the

site-site interactions than the bulk g(r) would be. This follows directly from the proportionality between the hard-wall contact density and pressure. As site-site attractions are "turned-on" the pressure and, consequently, the contact density is reduced. The density distribution becomes increasingly less sensitive to the site-site attractions as the distance is increased from the wall, and, of course, attractions between the wall and the polymer further complicate the system's response.

Here, we are interested in the study of inhomogeneous, purely repulsive, hard-site systems primarily because of the nature of our approach which centers about the direct correlation function, c(r), of the homogeneous system. Since the direct correlation function of attractive systems is often treated as an expansion about the c(r) of the repulsive system, the theoretical treatment of the underlying repulsive system needs to be understood in detail.

The general methodology for applying density functional theory to molecular systems was developed by Chandler, McCoy, and Singer [2] (CMS) and first applied to diatomics. Although its original application to diatomics used the direct correlation function as "input", it also encompasses the later molecular-DF theories that use the equation-of-state as input. For clarity, direct correlation function based approaches are referred to as CMS-DF theories, and equation-of-state based approaches as weighted-DF theories (WDF).

A number of previous, polymeric DF studies have taken place within the CMS formalism. The first "polymeric" application was a path-integral treatment of quantum helium[3]. This was followed by studies of rotational

isomeric state models of simple polymers[4,5]. The more complex phase behaviors of blends[6] and diblocks[7] were explored with simple tangent site models. Recent work[8] has investigated tangent site chains near walls with attractive "stripes". Finally, CMS-DF theory has been used[9] as the foundation for a theory of pair correlation functions in bulk molecular systems.

Weighted density functional (WDF) theories have also been applied to polymeric systems. The initial development of WDF theories for polymers was by Woodward[10] and Kierlik and Rosinburg[11]. More realistic, tangent site models were addressed by Yethiraj and Woodward[12], with an approach which has been more fully developed in a number of subsequent studies[13].

Both the structure and thermodynamics of the inhomogeneous system are predicted by DF theory. The structure arises from the two coupled equations:

$$\rho(\underline{r}) = G[U(\underline{r})] \tag{1.1}$$

and

$$U(\underline{r}) = U_E(\underline{r}) + U_M[\rho(\underline{r})] \tag{1.2}$$

where $\rho(r)$ is the inhomogeneous density. Here, $U(r)$ is an effective external field consisting of the "bare" external field, $U_E(r)$, and a medium induced external field, $U_M[\rho(r)]$. The functional, $G[U(r)]$, denotes a mapping of the external field onto the density where the brackets [...] indicate its functional nature. These equations, in general, must be solved

in a self-consistent manner. The free energy of the inhomogeneous system can then be expressed, in most cases, as a functional of the density and field.

The theoretical treatment, as presented here, is broad. If the medium induced potential is set to zero and U(r) is taken to include site-site interactions, then G becomes a full, many particle calculation with all its computational demands. The power of density functional theory is to simplify the calculations represented by G to those of a single particle calculation. For instance, the problem of many electrons in the external field created by a number of atomic nuclei is usually treated in a manner where G is the Schrodinger equation for a single electron in an external field. In other words, the electrons are treated by G as though there were no electron-electron interactions, and, consequently, the relatively complex $U_M(\underline{r})$ approximately corrects for energetic and statistical interactions between electrons.

An early precursor to DF theory has come to be known as Self Consistent Field (SCF) theory[14], although all density functional theories are, strictly speaking, also "self consistent field" theories. In SCF theory, the polymers are thread chains with the mapping functional G[U(r)] being, in effect, Schrodinger's equation. This makes computations relatively fast; however, the thread nature of the chain washes out most atomic level detail[15].

In order to retain such atomic level structure, Chandler, McCoy, and Singer[2] let G[U(r)] represent non-interacting molecules. This formalism permitted systems more complex than simple atoms to be

studied, and the method was made more general by the introduction[5] of the idea of using a Monte Carlo simulation of a single chain in an external field as a means of evaluating G[U(r)].

In the current study, polymer melts near hard walls are reexamined from the CMS perspective. Consequently, the direct correlation function, c(r), for the bulk polymer, which is in equilibrium with the inhomogeneous system, is used as "input". Loosely speaking, c(r) contains both equation of state and structural information. In particular, the k=0 component of the Fourier transform of c(r), $\hat{c}(0)$, is directly correlated with the system's isothermal compressibility which is an equation of state quantity. On the other hand, the rate of decay of c(r) introduces a length scale that has a strong influence on the particle correlations. In order to explore the structural consequences of c(r), various forms of c(r) were studied where $\hat{c}(0)$ was used to fix the compressibility and the resulting density profiles were compared.

The remainder of the paper is organized as follows. In section 2, the theoretical considerations introduced above will be elaborated upon. Details of the molecular model and solution techniques will be presented in section 3. Our results will be reported in section 4 and discussed in section 5. In the appendix, the related case of inhomogeneous hard sphere liquids is treated.

## 2. Theory

The density functional methodology employed here is based upon a second order expansion of the excess Helmholtz free energy of the

inhomogeneous system about the homogeneous system. It is important that an intelligent choice of the ideal system be used in the free energy expansion. This ideal system must be physically similar to the true system and, at the same time, "simple" to evaluate in both homogeneous and inhomogeneous states.

Many of the underlying complexities of DF theory arise from the need to evaluate the ideal system (non-interacting chains, in our case) at the same $\rho(r)$ as in the full system (i.e., not at the same external field). This necessitates the introduction of an ideal external field that can be expressed in terms of $\rho(r)$ through the minimization of the system's free energy. The density profile can then be found in a self-consistent manner. We have discussed the basic derivation of density functional theory in Paper I, and the interested reader is referred there for more details.

In previous work, (polymer reference interaction model – Percus Yevick) PRISM-PY liquid state theory was viewed as an inherent part of the method, forming a combined PRISM-DF theory, and the net accuracy of this approach was evaluated by comparisons with simulation and other theories. Such work[5,16] has demonstrated that the PRISM-DF theory yields accurate contact densities and profiles where, as shown in figure 1, deficiencies in PY-PRISM are compensated for by the (hypernetted chain) HNC type of field which comes directly from DF theory (see Paper I),

$$\beta U(\underline{r})_{M,HNC} = -\int c(|\underline{r} - \underline{r}'|)\Delta\rho(\underline{r}')d\underline{r}' \qquad (2.1)$$

where $\beta=1/k_B T$; T is the absolute temperature; and $k_B$ is the Boltzmann constant. The HNC form is exact for sufficiently small values of $\int c\Delta\rho$, but, as seen in figure 1, tends to over-predict the field strength at high bulk density when more correct liquid state input is used. Recently, other forms of the medium induced field have been suggested[9,17].

One of these suggested alternative fields with a weaker response to large values of $\int c\Delta\rho$ is the Percus-Yevick (PY) field:

$$\beta U(\underline{r})_{M,PY} = -\ln\left[1+\int c(|\underline{r}-\underline{r}'|)\Delta\rho(\underline{r}')d\underline{r}'\right] \qquad (2.2)$$

where the PY field is smaller than the HNC for large $c\Delta\rho$ values while approaching the HNC value for small values. This field type tends to be too weak.

The alternative field type that we consider which is intermediate between the HNC and PY types is the Martynov-Sarkisov (MS) field:

$$\beta U(\underline{r})_{M,MS} = -\sqrt{1+2\int c(|\underline{r}-\underline{r}'|)\Delta\rho(\underline{r}')d\underline{r}'}+1, \qquad (2.3)$$

which also guarantees that the HNC form will be recovered for small fields. A more general form proposed by Ballone et al.[18] permits one to interpolate between the MS and HNC forms; however, in the current study, this further refinement was not explored.

Unfortunately, in density functional applications, the operators present in all of the non-HNC fields can be problematic. When $\int c(|\underline{r}-\underline{r}'|)\Delta\rho(\underline{r}')d\underline{r}'$ falls below certain threshold values (for example, -1.0 for PY and -0.5 for MS), the fields fail to be real valued. In order to insure that simulation noise during the convergence process does not cause this line to be crossed, we switch to HNC fields when $\int c(|\underline{r}-\underline{r}'|)\Delta\rho(\underline{r}')d\underline{r}' = 0$.

Self-Consistent-Field theory uses a field similar to the HNC expression in equation (2.1); however, since the chains are of infinitesimal width, the c(r) becomes a delta function. This leads to an SCF-field of the form

$$\beta U(\underline{r})_{M,SCF} = -c_0\Delta\rho(\underline{r}) \tag{2.4}$$

where $c_0$ is the integrated value of $c(r)$. For this case the field is local in nature (although chain connectivity results in a non-local nature for the theory as a whole). The SCF-field does not see the density depletion due to the wall except as a boundary value issue, and, in addition, the length scale associated with the site diameter is non-existent. A typical result for this type of field is shown is figure 1. Of course, SCF theory is not constructed to model monomeric length scales, and it fails to capture the consequences of the site packing that results in the enhancement of site density near the wall.

Information is fed to CMS theory through the direct correlation function, c(r), which is a quantity containing a considerable amount of

information. The direct correlation function is closely associated with the equation of state through the isothermal compressibility

$$\kappa = \frac{1}{\rho}\left(\frac{\partial \rho}{\partial P}\right)_T = \frac{\beta N}{\rho\left(1 - N\rho\hat{c}(0)\right)} \tag{2.5}$$

where $\hat{c}(0)$ is the k=0 component of c(r)'s Fourier transform. If the compressibility is known as a function of density, the pressure can be found through integration; however, from this perspective, the pressure is not completely determined by the compressibility at a single density. It is intriguing that density functional theory permits the pressure to be found from the wall contact density, and this suggests that pressure can be found from the compressibility-dominated c(r) without the necessity of an integration over density.

In the current study, the direct correlation function is found in a number of ways, some more approximate than others. First, polymer reference interaction site model (PRISM) theory is used. The generalized Ornstein-Zernike equation, which can be viewed as defining c(r), is given by

$$h(r) = \omega * c * \omega(r) + \rho\omega * c * h(r) \tag{2.6}$$

where "*" indicates a convolution integral; h(r)=g(r)-1; g(r) is the inter-chain pair correlation function; and $\omega(r)$ is the intra-chain pair correlation

function. The $\omega(r)$'s used were found from Monte Carlo simulations of pearl necklace chains. In figure 2, the Fourier transform of this correlation function, $\hat{\omega}(k)$, is shown for various densities along with that of a freely jointed chain. For densities over 0.668, the $\omega(r)$ is assumed to be independent of density.

For the case of hard sites, the (Percus-Yevick) PY closure collapses to

$$\begin{aligned} g(r) &= 0 \quad \text{for } r < \sigma \\ c(r) &= 0 \quad \text{for } r \geq \sigma \end{aligned} \tag{2.7}$$

where the direct correlation calculated through this "uncorrected PY" closure will be referred to a $c_{PY}(r)$, and where the $\omega(r)$ was evaluated from Monte Carlo simulations of pearl-necklace melts. Using this closure with an HNC-DF theory yields excellent agreement with simulation; however, the compressibility is not well described by $\hat{c}(0)$ through the relation (2.5).

In the current study, we insist that $\hat{c}(0)$ be consistent with the isothermal compressibility that is found through the equation of state. This condition is enforced in a number of ways. First, $c_{PY}(r)$ is multiplied by a constant yielding a "corrected PY" closure and, unless otherwise indicated, "PY" will denote this corrected form. Second, a tail function[19] is added to $c(r)$ outside the core of the form

$$\begin{aligned} g(r) &= 0 && \text{for } r < \sigma \\ c(r) &= c(\sigma^-)\left(\frac{\sigma}{r}\right)^x && \text{for } r \geq \sigma \end{aligned} \tag{2.8}$$

with x varied after each PRISM iteration to force the c(r)'s integrated value to be consistent with its equation of state value.

In order to gauge the relative importance of c(r)'s integrated value as compared to that of its detailed structure; we have also looked at a number of simplified c(r)'s. The simplest of these is a square well c(r) where

$$\begin{aligned} c(r) &= \frac{3\hat{c}(0)}{4\pi\sigma^3} && \text{for } r \leq \sigma \\ c(r) &= 0 && \text{for } r > \sigma \end{aligned} \tag{2.9}$$

Nearly as straightforward is a "slant" c(r) given by

$$\begin{aligned} c(r) &= \frac{3\hat{c}(0)}{\pi\sigma^3}\left(1-\frac{\sigma}{r}\right) && \text{for } r \leq \sigma \\ c(r) &= 0 && \text{for } r > \sigma \end{aligned} \tag{2.10}$$

## 3. Chain Models and Solution Method

The density functional calculations in the current study are intended to mimic the inhomogeneous density profiles which result from the presence of a hard wall on a melt of hard 20-mer, pearl-necklace chains at varying densities. At all densities, the density profile, $\rho(z)$, at contact is related to the pressure, P, by[20]

$$\rho(z=0) = \beta P \tag{3.1}$$

where $\rho(z)$ is the inhomogeneous *site* density. Far from the wall the density adopts its bulk value, $\rho_{bulk}$. At low densities, the density will increase gradually to $\rho_{bulk}$ over a distance equal to roughly the chain's radius of gyration. As the density of pearl necklace chains increases, oscillations develop in $\rho(z)$ with a period of roughly the hard site diameter; however, as the chain backbone becomes more complex, other length scales are introduced which are evidenced[5] in $\rho(z)$.

In the ideal gas limit, the pressure will be related to the density far from the wall by

$$\frac{\rho_{bulk}}{N} = \beta P \tag{3.2}$$

where N is the chain length and $(\rho_{bulk}/N)$ is the molecular density. From equations (3.1) and (3.2) it is clear that in the low density limit, the ratio of contact to bulk densities approaches 1/N:

$$\frac{\rho(0)}{\rho_{bulk}} = \frac{1}{N}. \tag{3.3}$$

For all chains in the current study, the bond length, $\ell$, is rigid and is equal to the site diameter. Consequently, $\sigma$ is taken as the unit length in our study, $\ell=\sigma=1$. No bond angle potentials are imposed, and, consequently, the chains should be viewed as freely jointed to within the restrictions of the non-bonded, site-site potentials. For the pearl-necklace

(PN) chain model, these non-bonded, intra-chain interactions function to exclude overlap between any two sites on the chain:

$$\begin{aligned} U(r_{\alpha,\gamma}) &= \infty \quad r_{\alpha,\gamma} < \sigma \quad (\alpha \neq \gamma) \\ U(r_{\alpha,\gamma}) &= 0 \quad r_{\alpha,\gamma} \geq \sigma \quad (\alpha \neq \gamma) \end{aligned} \tag{3.4}$$

where $U(r_{\alpha,\gamma})$ represents the energy for sites with a distance $r_{\alpha,\gamma}$ between the $\alpha^{th}$ and the $\gamma^{th}$ site on the chain.

The equation of state for pearl-necklace chains has been investigated by Chang and Sandler[21] for chain lengths up to 16 sites; by Escobedo and dePablo[22] for 16, 32, and 51 site chains; and by Stell et al.[23] for 51 and 201 site chains. In figure 3, an interpolation of these results to 20-site chains is shown. The interpolation is fit to the empirical function

$$\beta P = \rho\left(\frac{1}{N}\exp\left(A(\rho/\sigma)^B\right)\right) \tag{3.5}$$

where A=5.4267, and B=0.73858. This yields a relationship for the compressibility, $\kappa$,

$$\kappa = \frac{\beta}{\rho}\left[\frac{1}{N}\exp\left(A(\rho/\sigma)^B\right)\left(AB(\rho/\sigma)^B + 1\right)\right]^{-1} \tag{3.6}$$

and, consequently, of the k=0 value of the Fourier transform of the direct correlation function, $\hat{c}(0)$,

$$\hat{c}(0) = \frac{1}{N\rho} - \frac{\beta}{\rho^2 \kappa} \tag{3.7}$$

Also shown in figure 3, are equation of state points found from contact densities in simulations of 20-site chains[12,13] near hard walls. For high densities, these simulations become difficult and the error bars are increased. Over the entire range of densities of interest, equation (3.5) is in excellent agreement with extrapolations from the equation of state developed by Escobedo et al.[22] for similar systems.

In a melt of pearl-necklace chains, excluded volume interactions are screened out resulting in random walk scaling on long length scales ($R_g \sim N^{1/2}$). As the density is reduced, this distribution crosses over to that of a self-avoiding random walk where $R_g \sim N^{3/5}$. In order to capture the effect of the medium on the single-chain distribution function within density functional theory, we have used three types of ideal chains: the full pearl-necklace, the second nearest neighbor, and the freely jointed chain models.

The pearl-necklace (PN) chain would best model low-density melts and perhaps, chains in the vicinity of the wall. The second nearest neighbor (NN) chains differ from PN chains in terms of their non-bonded interactions, where equation (3.4) is replaced by

$$\begin{aligned} U(r_{\alpha,\alpha+2}) &= \infty \quad r_{\alpha,\alpha+2} < \sigma \\ U(r_{\alpha,\alpha+2}) &= 0 \quad r_{\alpha,\alpha+2} \geq \sigma \end{aligned} \tag{3.8}$$

where $U(r_{\alpha,\alpha+2})$ represents the energy for sites with $r_{\alpha,\alpha+2}$ distance between the $\alpha^{th}$ and the $(\alpha+2)^{th}$ site on the chain. These chains would be expected to model a melt reasonably well since the random-walk nature of the chains would be maintained far from the wall while local chain collapse would be avoided. Finally, the freely jointed (FJ) chains have no excluded volume restrictions, and, consequently, would be expected to be the least capable of modeling a melt of PN chains. On the other hand, FJ chains are similar to the ideal chain models used in SCF theories, which, if for no other reason, make FJ chains of interest in the current study.

The iterative process is begun with the assumption of an initial density profile on a grid spacing of $0.004\sigma$; an initial field is calculated from this density profile, equation (1.2) and one of the field relations given by equations (2.1) to (2.4). An iterative loop is then begun wherein the site density is found from the average over position in a single chain simulation under the previously calculated external field. Each simulation takes place between two atomically smooth hard walls, positioned perpendicular to the z-axis, and separated by a distance of $20\sigma$. Since the walls are invariant in both the x and y-directions, the chain is re-centered within the x and y-directions periodically during the simulation.

For all data presented here, the initial density profile is chosen to be constant at $\rho_{bulk}$ to begin the lowest density run. Subsequently, the final converged profile is rescaled from the previous density to the current

density, and equilibration then takes place from this point. For moderate packing fractions (generally, $\eta \leq 0.30$), a high level of convergence is reached within approximately 50 iterations of $10^6$ samples each. As the packing fraction rises, however, substantially more samples are necessary in order to reduce the simulation noise inherent in the higher field calculations.

Over the course of the simulation, statistics are collected, on a site-by-site basis, which represent the density profiles of the chain as it moves between the hard walls, constrained by the model-specific potential interactions as well as the bulk-field energies of our DF theory. Monte Carlo moves are accomplished through both translation and reptation moves. The reptation moves are simple in nature, consisting of the removal of a single site from one end of the chain model and its reattachment to the complementary end. Translation moves are limited to a maximum of $2.0\sigma$ in either the positive or negative z-direction. The number of attempted moves is equivalent to $N^2$ times the number of samples desired (e.g., for the $10^6$ samples above, our 20-mer has $400 \times 10^6$ attempted moves). Of these moves, 15% are translation, with the remaining moves being split equally among left-hand and right-hand reptations.

As discussed in Paper I, the Metropolis weighting of each move is determined with respect to the external, umbrella field

$$U(z) = U_E(z) + U_U(z) \tag{3.9}$$

where

$$\beta U_U(z) = a\left(\frac{z - z_{center}}{z_{center}}\right)^4 ; \qquad (3.10)$$

$z_{center}$ is halfway between the walls; and a is an empirical constant (a=-0.40 for this work) chosen to enhance sampling. This forces the chains to spend much of their time near the walls where good statistics are essential to the convergence of the density functional theory. For atomic hard spheres, the calculation is, of course, much simpler as is discussed in the appendix.

After the completion of a full iteration, density statistics are first averaged about the middle of the profile and are then rescaled to achieve the correct bulk density within the middle 10% of the density profile. Once this has been done, a new field is calculated from this "simulated" density. To help maintain the stability of the iteration scheme, the density profile is found by mixing 15% of the simulated profile with 85% of the old profile. The field calculated from this new profile is mixed in a 1/99 ratio with the old field to generate the new field for the next iteration. These percentages are slightly modified based on the current percentage of iterations completed or the current standard deviation between the raw old and new profiles in an effort to promote initial equilibration and hinder divergence due to large-scale noise, respectively. These numbers were arrived at empirically, and must be carefully monitored. If necessary, they must be adjusted in order to allow successful convergence, especially with fields

containing high magnitude field differences. Insufficient sampling or over-mixing of the new profiles with the old leads to wildly oscillatory fields which have difficulty converging, while under-mixing of the new profiles can lead to false or excessively slow convergence.

## 4. Results

There are several phenomena of interest which have been noticed over the course of this work. Foremost among these is the ability to specify the contact density through specification of c(r)'s integrated value, $\hat{c}(0)$. Figure 4 presents the pressures predicted through equation (3.1) and our implementation of CMS DF theory, overlaid on the 20-mer equation of state presented in figure 3, from which our compressibility values were derived. The quality of agreement between the equation of state and our calculations for $\eta \leq 0.35$ is excellent, provided the MS form for the mean induced field is employed. Employment of the HNC mean induced field leads to pressures which are substantial over estimations, while the PY mean induced field leads to pressures which are under estimations. While our equation of state calculations stray from the bulk equation of state for packing fractions above 0.35, so too does the equation of state derived from the Monte Carlo simulations by Yethiraj. These difficulties may be related to the confinement of the chain between the hard walls and subsequent induced pressure differences, or they may simply be due to the extreme difficulty of extrapolating a correct value for $\rho(z=0)$ at higher densities where there is a precipitous rise in density near wall contact.

The DF calculation turns out to be less sensitive to the nature of the chain model used in the DF calculation to mimic the full excluded volume of the true (i.e., pearl necklace) chain than we had anticipated. The inhomogeneous density profiles are identical for calculations employing either PN or NN chain models, while, on the other hand, the FJ chain model shows substantially lower pressures at higher densities.

Although there seems to be little difference between the PRISM-PY and "slant" forms for $c(r)$, at least as they relate to the overall system pressure, the square-well form shows a sharp drop in pressure at higher densities. This is likely due to the longer range (see figure 10) of the interaction field, leading to significantly greater propagation of field interactions. For the square-well potential, visible density fluctuations extended into the central region of the cell (at which bulk conditions are explicitly assumed) at packing fractions as low as 0.40 ($\rho\sigma^3 = 0.764$). By comparison, all other forms for $c(r)$ avoided this problem until the packing fraction neared 0.50 ($\rho\sigma^3 = 0.955$). Whether this drop in pressure is a real feature of the system or a consequence of violating the initial assumption of a bulk liquid region in the center is currently unexplored.

While the form of $c(r)$ employed seems to differentiate between experimental pressures only at high densities, there is a more pronounced effect of the differing forms of $c(r)$ on the density profiles, even at moderate densities, as shown in figures 5 and 6. Figure 5 demonstrates the substantial differences between the density profiles generated with differing functional forms for $c(r)$, while figure 6 compares the "slant",

PRISM-PY, and PRISM-Tail generated profiles to observations of full simulations.

Here, it can be clearly seen that the slant, PRISM-PY, and PRISM-Tail forms for $c(r)$ yield reasonably similar results, while those of the square-well form differ significantly. While the PRISM-Tail $c(r)$ seems to fit the experimental data best overall, the "slant" form does a good job of capturing the quantitative details of the simulation data. Both curves suffer from a slight out of phase character, with the "slant" form being more pronounced. As well, both forms yield a slight underestimation of the depth of the initial trough and a slight overestimation of the height of the first peak from the wall. For reference, figure 7 compares our results utilizing the corrected PRISM-Tail $c(r)$ and MS field to both the simulation and WDA results found by Yethiraj[13] at a relatively high density. We find our results to be of similar quality to that obtained with current WDA techniques.

The overall quality of the density profile is dictated not only by the functional form chosen for $c(r)$, but also by the mean induced field type employed as well. While the most significant effect is that exhibited by the field type's effect upon the contact density, it is also exhibited in the secondary and higher order density oscillations present as the polymer relaxes to its bulk behavior. Figure 8 presents a schematic wherein two significant features are noticeable: foremost, the HNC field predicts a significantly higher contact density than does either the MS or PY field, even for moderate densities. Additionally, at moderate distances from the wall, the HNC field yields higher absolute values for the higher order

density peaks and troughs, as well as locating such features at somewhat closer approaches to the hard wall. While the PY and MS fields differ somewhat in their predictions for contact density, with the MS being slightly higher than the PY, both fields quickly settle into long range profiles that are nearly identical.

To ensure that such features arise strictly from the field type chosen, rather than from a combination of field type and compressibility constraints, the profile of a compressibility corrected and uncorrected system, utilizing the PRISM-PY form for $c(r)$, are presented in figure 9. The results presented indicate that enforcing the correct value of $\hat{c}(0)$ has little effect on the location of the density profile features of interest, while having a noticeable effect on the amplitude of these features.

To understand the origin of the phase invariance found through scaling the direct correlation function, the different forms of $c(r)$ must first be explored. Figure 10 presents the four major $c(r)$ types employed within this work. While most of these forms of $c(r)$ look distinctly different from each other in this figure, it should be noted they all possess the same $\hat{c}(0)$. The insert, on the other hand, presents the same functions plotted as $r^2c(r)$ so that the areas under the curves are directly proportional to $\hat{c}(0)$. Consequently, the characteristic length scale in the direct correlation functions is apparent when plotted in this manner.

In most cases, the change in $\hat{c}(0)$ is accomplished through simple constant scaling of the direct correlation function. This leads to results wherein only the relative amplitude of the minima seen in the insert to

figure 10 are affected, while their location in terms of displacement from the $r = 0$ core of the particle remain unchanged. This is important, since the location of these minima appear to set an effective length scale for the functioning of the density functional theory. Thus, the form of the $c(r)$ function controls the length scale of interactions between sites, and, to some extent, the strength of these interactions as well. The overall value of $\hat{c}(0)$, on the other hand, serves as a type of "fine-tuning" control to adjust the strength of these interactions, while having no significant impact on the interaction length scale. Of particular interest when comparing the different forms of $c(r)$, and their eventual outcome, is the fact that the "slant", PRISM-PY, and PRISM-Tail all have qualitatively similar features when viewed as $r^2c(r)$, while the square-well form is distinctly different.

The above arguments are not true for the PRISM-Tail form of $c(r)$, due to the overall value of $\hat{c}(0)$ being enforced not by multiplication, but, instead, by self-consistent adjustment to the radial power of the tail. Nevertheless as the density of the liquid system increases, the PRISM-Tail exponent rises rapidly. Thus, at moderately high densities, the PRISM-Tail form for $c(r)$ becomes increasingly similar to the PRISM-PY form with corrected $\hat{c}(0)$, with similarly located density fluctuations and only small differences in density amplitudes, as can be seen in figure 9.

Investigations show that the system is largely insensitive to differences in the intra-chain volume exclusion interactions. While the freely jointed chain does indeed show a lowering of overall system pressure, this does not seem to correspond to a large-scale difference in

overall profile. It should be noted, however, that while the density profiles seem relatively insensitive to the changes in the intra-chain interactions, the equation of state (figure 4) shows quantitative differences between the chain types. Of particular interest is the fact that the equation of state for the freely jointed chain differs significantly, while the overall profile differs little. Also of interest is the slight phase compression exhibited by the freely jointed chain, which appears to be the result of the extreme compressibility of the chains near the hard wall surface.

## 5 Discussion

Several conclusions immediately follow from the data presented herein. Foremost among these is the ability of the pressure of the system to be primarily specified by employing the correct value of $\hat{c}(0)$. Deviations, which occur due to the functional form employed for $c(r)$, represent small percentages of the overall equation of state, provided the assumption of bulk phase equilibrium at the center of the cell is not violated. While this may seem to be similar to the WDA theory discussed above, it obviates the need for a complete equation of state to perform DF theory calculations that yield the correct bulk pressure. Instead, a single compressibility measurement of the system in question will suffice to allow control of the bulk pressure. This is of special importance in the case of molecules with multiple types of sites, where the calculation of site-specific equations of state makes WDA approaches problematic. Of course, if the exact c(r) is available, either from theory, simulation, or experiment, an equation of state is not necessary for accurate DF predictions.

Along with careful attention to the field type, care must also be paid when employing a specific functional form of $c(r)$. Obviously, the best choice for the form of $c(r)$ would be a directly calculated value, but this is often difficult. Instead, we have found that both PRISM-PY (with appropriate scaling to enforce the correct value for $\hat{c}(0)$) and PRISM-Tail approaches to calculation of $c(r)$ yield quite good results. Further, for quick exploratory calculations, the "slant" function as presented herein shows reasonably good agreement with simulation profiles, while representing a significant computational savings from the PRISM calculations. In addition, the slant c(r) is a simple two parameter ($\hat{c}(0)$ and site diameter) model which is reasonably realistic.

The effect of the intra-chain constraints on the pressure and excess free energy of the system can be understood by considering the degree to which the chains can respond to the conformational restrictions introduced by the wall. In the case of the freely jointed chain the entropic reduction engendered by the hard wall boundary conditions is significantly lessened due to the chain's ability to pack multiple sites within the same space. Since the pearl necklace chain *must* exclude sites from within the hard core of other sites, the overall effect upon the system is that of greater suppression of entropic freedom than encountered in the freely jointed system. Thus, the overall effect is a higher pressure for the pearl necklace system (due to the inability of the chain to collapse in the high-density region near wall contact).

Interestingly, the nearest neighbor chain is much more similar to the pearl necklace chain in its pressure than it is to the freely jointed chain. This, in turn, implies that, for the chains investigated here, the primary interaction of importance is the volume exclusion between the primary ($\alpha^{th}$) and tertiary ($\alpha$+2)$^{th}$ sites. This is not surprising since similar behavior was observed earlier in the self-consistent PRISM work of Schweizer et al.[24]. On the other hand, the importance of this difference is obviously a function of density, as increasing densities cause the sites to be packed increasingly closer, leading to an increase in non-primary interactions, and subsequent differentiation between a model which enforces only the primary interaction and one which enforces all interactions.

## Appendix: The Atomic Hard Sphere Case

As one would expect, the application of the procedures in the body of the paper to the atomic hard sphere case results in great simplifications. For comparative purposes, the hard sphere case is of interest to the current study. Qualitatively, the conclusions drawn for the polymer case also hold for the atomic case.

The equations necessary for Hard Spheres follow. The relationship G[U(r)] in equation (1.1) simplifies to

$$\rho(z) = \rho_{bulk} \exp[-\beta U(z)] \tag{A.1}$$

and, as a result, no simulation (or umbrella field) is required. The Carnahan-Starling equation of state[25] is

$$\frac{\beta P}{\rho} = \frac{1+\eta+\eta^2-\eta^3}{(1-\eta)^3}. \tag{A.2}$$

The PY solution for the direct correlation function[25] is

$$c(r) = -\lambda_1 - 6\eta\lambda_2 r - 0.5\eta\lambda_1 r^3 \tag{A.3}$$

where

$$\lambda_1 = \frac{(1+2\eta)^2}{(1-\eta)^4} \tag{A.4}$$

and

$$\lambda_2 = -\frac{(1+0.5\eta)^2}{(1-\eta)^4}. \tag{A.5}$$

The k=0 component of the Fourier component of the direct correlation function as found from the equation of state is

$$\hat{c}_{cs}(0) = \frac{\pi(2\eta-9)}{6(1-\eta)^4} \tag{A.6}$$

and, from the PY solution,

$$\hat{c}_{PY}(0) = \frac{\pi\left(\eta^3 - 4\eta^2 + 2\eta - 8\right)}{6(1-\eta)^4}. \tag{A.7}$$

The partial integration of c(r) over x and y is, for the PY case,

$$C_{PY}(z) = \pi\left[-\lambda_1\left(1-z^2\right) - 4\eta\lambda_2\left(1-|z|^3\right) - \frac{\eta\lambda_1}{5}\left(1-|z|^5\right)\right]; \tag{A.8}$$

for the slant case,

$$C_{Slant}(z) = \hat{c}(0)\left[1-3z^2+2|z|^3\right]; \tag{A.9}$$

and, for the square well case,

$$C_{SqWell}(z) = \hat{c}(0)\frac{3}{4}\left[1-z^2\right]. \tag{A.10}$$

As for the polymer case, the wall contact densities (or pressures) are insensitive to the shape of the direct correlation function. This relationship held even for cases where the densities were otherwise dissimilar. In figure A.1 it is shown that the MS field type gives an excellent description for the equation of state for hard sphere liquids. Although, the slant results are shown, the PY and square well give, to within numerical noise, identical contact values. It is of particular interest to note that slant density profiles become crystal-like with periodic structure bridging between the wall for densities above about 0.95.

**References**


1) J.B. Hooper, J. D. McCoy, and J. G. Curro, J. Chem. Phys. (preceding paper).

2) D. Chandler, J. D. McCoy, S. J. Singer, J. Chem. Phys. **85**, 5971 (1986); Ibid, **85**, 5977;J. D. McCoy, S. J. Singer, D. Chandler, J. Chem. Phys. **87**, 4853 (1987).

3) S. W. Rick, J. D. McCoy, and A. D. J. Haymet, *Chemical Applications of Density Functional Theory*, ed. B. B. Laird, R. B. Ross, and T. Ziegler (American Chemical Society, Washington, 1996), 286; J. D. McCoy, S. W. Rick and A. D. J. Haymet, J. Chem. Phys. **90**, 4622 (1989); J. D. McCoy, S. W. Rick and A. D. J. Haymet , *ibid.* **92**, 3034 (1990); S. W. Rick , J. D. McCoy and A. D. J. Haymet, *ibid.* **92**, 3040 (1990).

4) J. D. McCoy, K. G. Honnell, K. S. Schweizer, and J. G. Curro, J. Chem. Phys. **95**, 9348 (1991).

5) S. Sen, J. M. Cohen, and J. D. McCoy, J. Chem. Phys. **101**, 3205 (1994); S. Sen, J. D. McCoy, S. K. Nath, J. P. Donley, and J. G. Curro, J. Chem. Phys. **102**, 3431 (1994).

6) S. K. Nath, J. D. McCoy, J. G. Curro, and R. S. Saunders, J. Polym. Sci. B:Polym. Phys. **33**, 2307 (1995).

7) S. K. Nath, J. D. McCoy, J. G. Curro, and R. S. Saunders, J. Chem. Phys. **106**, 1950 (1997); J. D. McCoy, S. K. Nath, J. G. Curro, and R. S. Saunders, J. Chem. Phys. **108**, 3023 (1998).

8) S. K. Nath, P. F. Nealey, and J. J. de Pablo, J. Chem. Phys. **110**, 7883 (1999).

9) J. P. Donley, J. G. Curro, and J. D. McCoy, J. Chem. Phys. **101**, 3205 (1994).

10) C. E. Woodward, J. Chem. Phys. **94**, 3183 (1991).

11) E. Kierlik and M. L. Rosinberg, J. Chem. Phys. **100**, 1716 (1994).

12) A. Yethiraj and C. E. Woodward, J. Chem. Phys. **102**, 5499 (1995).

13) A. Yethiraj, Chemical Applications of Density Functional Theory, ed. B. B. Laird, R. B. Ross, and T. Ziegler (American Chemical Society, Washington, 1996), 274; A Yethiraj, J. Chem. Phys. **109**, 3269 (1998); A. Yethiraj, Chem. Eng. Journal 74, 109 (1999).

14) E. Helfand and Y. Tagami, J.Polym. Sci. B **9**, 741 (1971); J. Chem. Phys. **56**, 3592 (1971); *ibid.* **57**, 1812 (1972); E. Helfand and Z. R. Wasserman, Macromolecules **9**, 879 (1976); *ibid.* **11**, 960 (1978); *ibid.* **13**, 994 (1980); Polym.Eng. Sci. **17**, 535 (1977).

15) S. K. Nath, J. D. McCoy, J. P. Donley, and J. G. Curro, J. Chem. Phys. **103**, 1635 (1995).

16) J. D. McCoy, and S. K. Nath, *Chemical Applications of Density Functional Theory*, ed. B. B. Laird, R. B. Ross, and T. Ziegler (American Chemical Society, Washington, 1996),

17) C. J. Grayce and K. S. Schweizer, J. Chem. Phys. **100**, 6846 (1994).

18) P. Ballone, G. Pastore, G. Galli, and D. Gazzillo, Mol. Phys. **59**, 275 (1986).

19) J.G. Curro, E. B. Webb III, G. S. Grest, J. D. Weinhold, M. Puetz, J. D. McCoy, J. Chem. Phys. (in press).

20) J. L. Lebowitz, Phys. Fluids **3**, 64 (1960); J. K. Percus, J. Stat. Phys. **15**, 423 (1976); R. Dickman and C.K. Hall, J. Chem. Phys. **89**, 3168 (1988).

21) J. Chang and S. I. Sandler, Chem. Eng. Sci. **49**, 2777 (1993).

22) F. A. Escobedo and J. J. dePablo, J. Chem. Phys. **102**, 2636 (1995); J. Chem. Phys. **103**, 1946 (1995);

23) G. Stell, C.-T. Lin, Yu. V. Kalyuzhnyi, J. Chem. Phys. **110**, 5458 (1999).

24) K. S. Schweizer, K.G. Honnell, J. G. Curro, J. Chem. Phys. **96**, 3211 (1992).

25) J. P. Hansen and I. R. McDonald, Theory of Simple Liquids (Academic Press, New York, 1986).

## Figure Captions

1) Comparisons of DF theory (lines) to full simulations[13] (symbols). The upper set of results is at a bulk density of 0.830 and have been shifted by +1 for clarity. The lower set is at a bulk density of 0.642. The solid line is uncorrected PRISM-PY input with an HNC field. The long dashed line is corrected PRISM-PY with an HNC field. The short dashed line is corrected PRISM-PY with a SCF field.

2) Comparison of ideal (solid line) and bulk simulated $\omega(k)$ for differing densities. ($\rho_{Bulk}$=0.211 long dash, $\rho_{Bulk}$=0.381 short dash, $\rho_{Bulk}$=0.642 dotted) The large k region is blown-up in the insert.

3) Equation of state for differing chain sizes. The inverted triangles are from bulk liquid simulations for chains of 16 sites, and the triangles, for 32 sites. The crosses are from simulations[13] of 20 site chains between hard walls 20$\sigma$ apart.

4) Equation of state for differing field types. Three groupings of data are considered, each offset by +3 for clarity. The top compares field types; the middle, c(r) types; and the bottom, chain backbone types. The solid line is the interpolation of bulk liquid equation of state data[21,22]; the dashed line is equation of state data from simulations near a hard wall[13]. The filled diamonds are the slant c(r) with MS field type and NN chain backbone results. The triangles are slant-c(r), HNC-field, NN-chain results; and the inverted triangles are slant-c(r), PY-field, NN-chain results. The open diamonds are PRISM-tail-c(r), MS-field,

NN-chain results; and the squares are straight-c(r), MS-field, NN-chain results. The crosses are slant-c(r), MS-field, PN-chain results; and the circles are slant-c(r), MS-field, FJ-chain results. Results below $\rho_{Bulk}$=0.70 are highly overlapped.

5) The effect of the form of c(r) on the density profiles. All calculations are for MS fields and NN chains, and occur at $\rho_{Bulk}$=0.642. (Solid line – PRISM-PY corrected, Dashed line – "Slant", Dotted line – Square well).

6) Comparison of Monte Carlo simulations[13] (symbols) with our DF results. For clarity, the $\eta$=0.43 curve has been shifted up by 0.5. All calculations are for MS fields and NN chains (Solid – PRISM-PY, Dashed – "Slant", Dotted – PRISM-Tail). Bulk densities are 0.211, 0.381, 0.642, and 0.830.

7) Comparison of CMS DF theory (solid line) to WDA DF theory (dashed line) and Monte Carlo simulations[13] [13 ] (circles). CMS DF calculation is for an MS field, PRISM-Tail form of c(r), and NN chains. The square is extracted from the equation-of-state interpolation. All values are for $\rho_{Bulk}\cong$0.830.

8) Effect of differing field types on the density profile. (Dotted line – HNC, Solid line – MS, Dashed line – PY). All calculations are for slant-c(r)'s and NN chains. All simulations are at $\rho_{Bulk}$=0.830.

9) Effect of compressibility corrections on the density profile. (Dot-dashed – PRISM-PY corrected, Dotted line – PRISM-PY uncorrected, Solid line- PRISM-tail ). The symbols are for the full simulation. All calculations are for MS fields and NN chains. All values are for $\rho_{Bulk}$=0.830.

10) Differing forms of c(r) in linear space. While the slant (long dashes) and square well (solid line) differ decidedly, the PRISM-PY corrected (dotted line) and PRIMS-Tail (short dashes) are quite similar. All values are from calculations at $\rho_{Bulk}$=0.830. The insert shows the c(r)'s times the volume element, $r^2$.

A.1) The Carnahan-Starling equation of state of hard spheres (line) is exactly reproduced by the MS field with a "slant" c(r) (filled circles) as contrasted with the HNC field of the same c(r) (open circles).

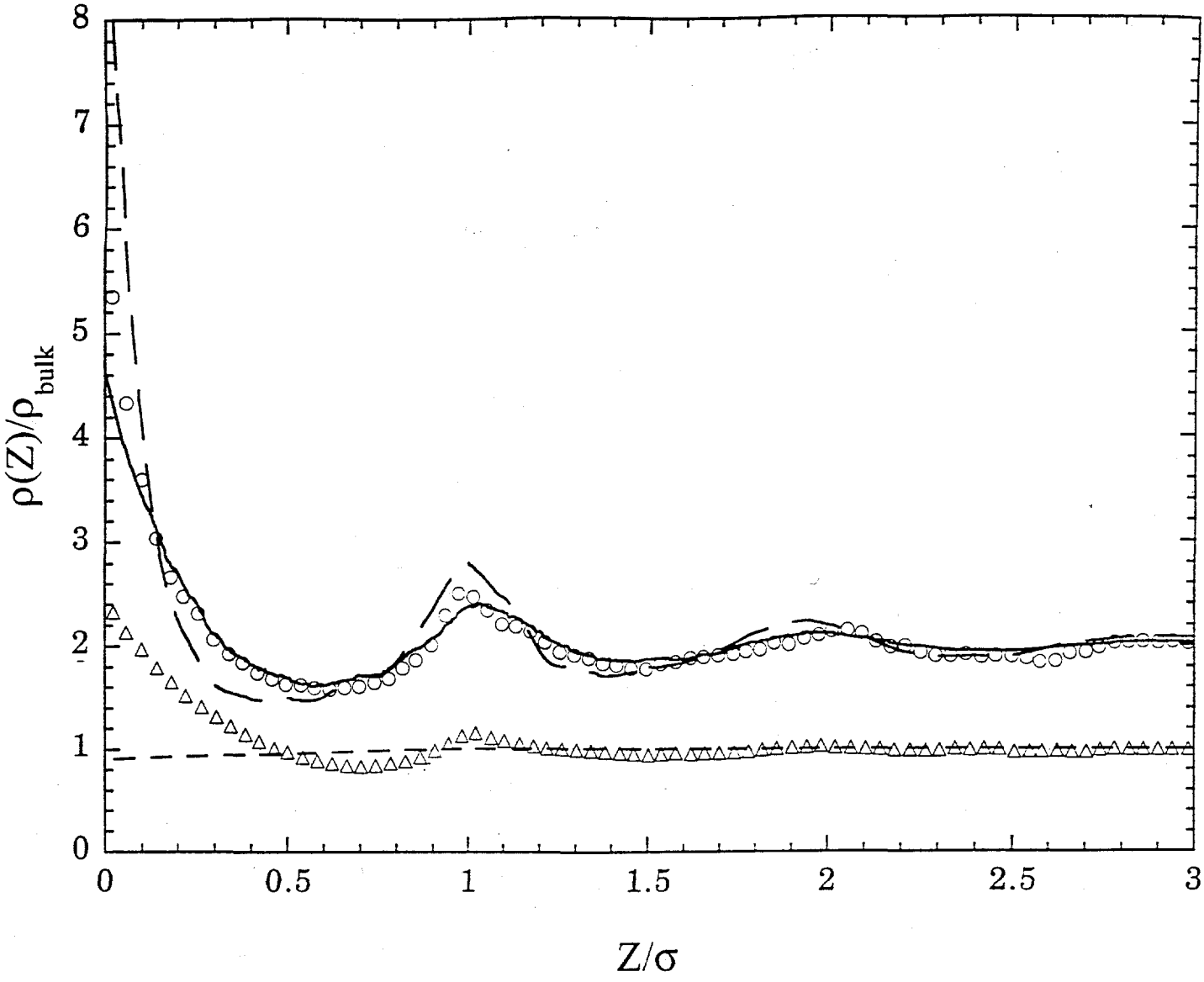


Figure 1

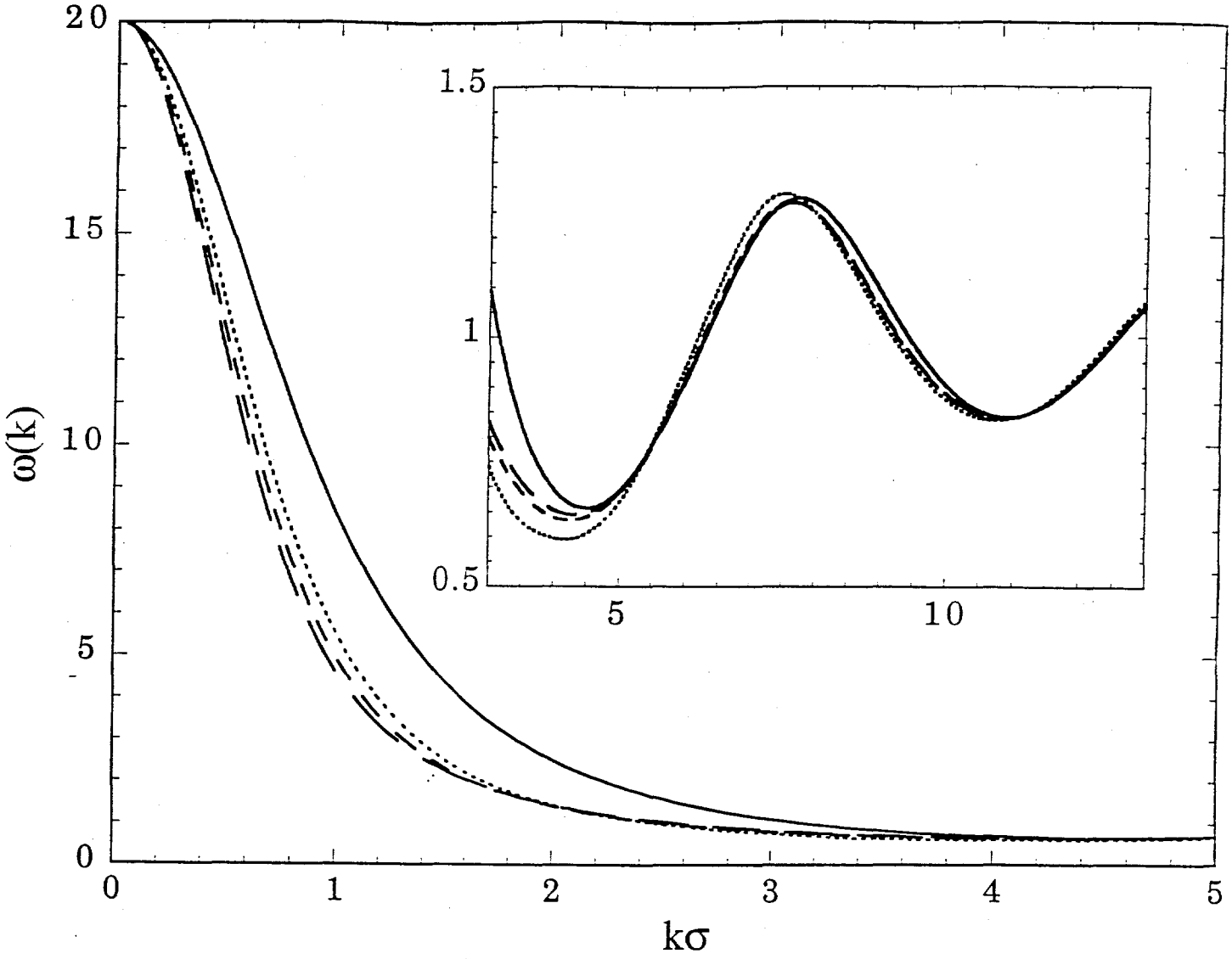


Figure 2

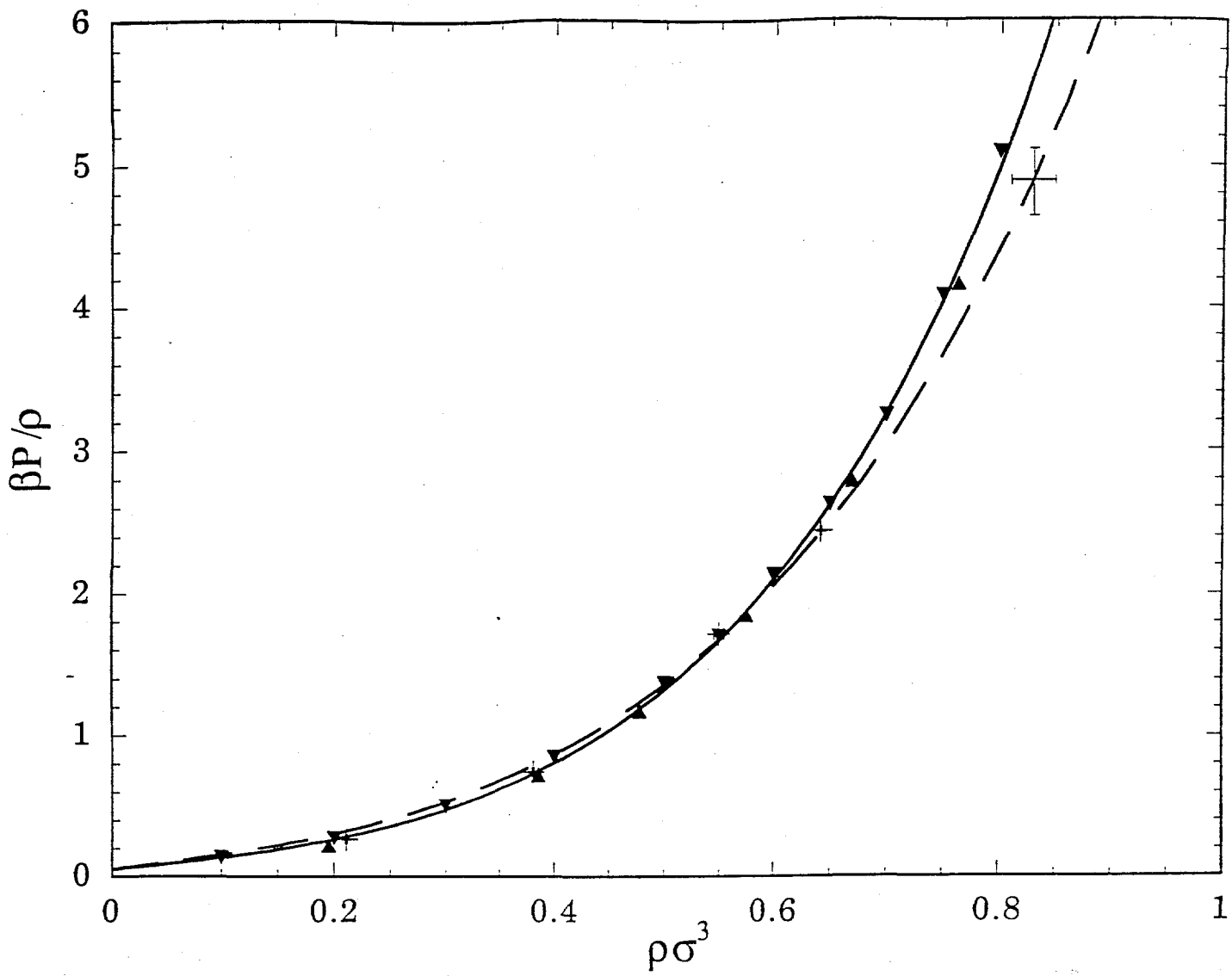


Figure 3

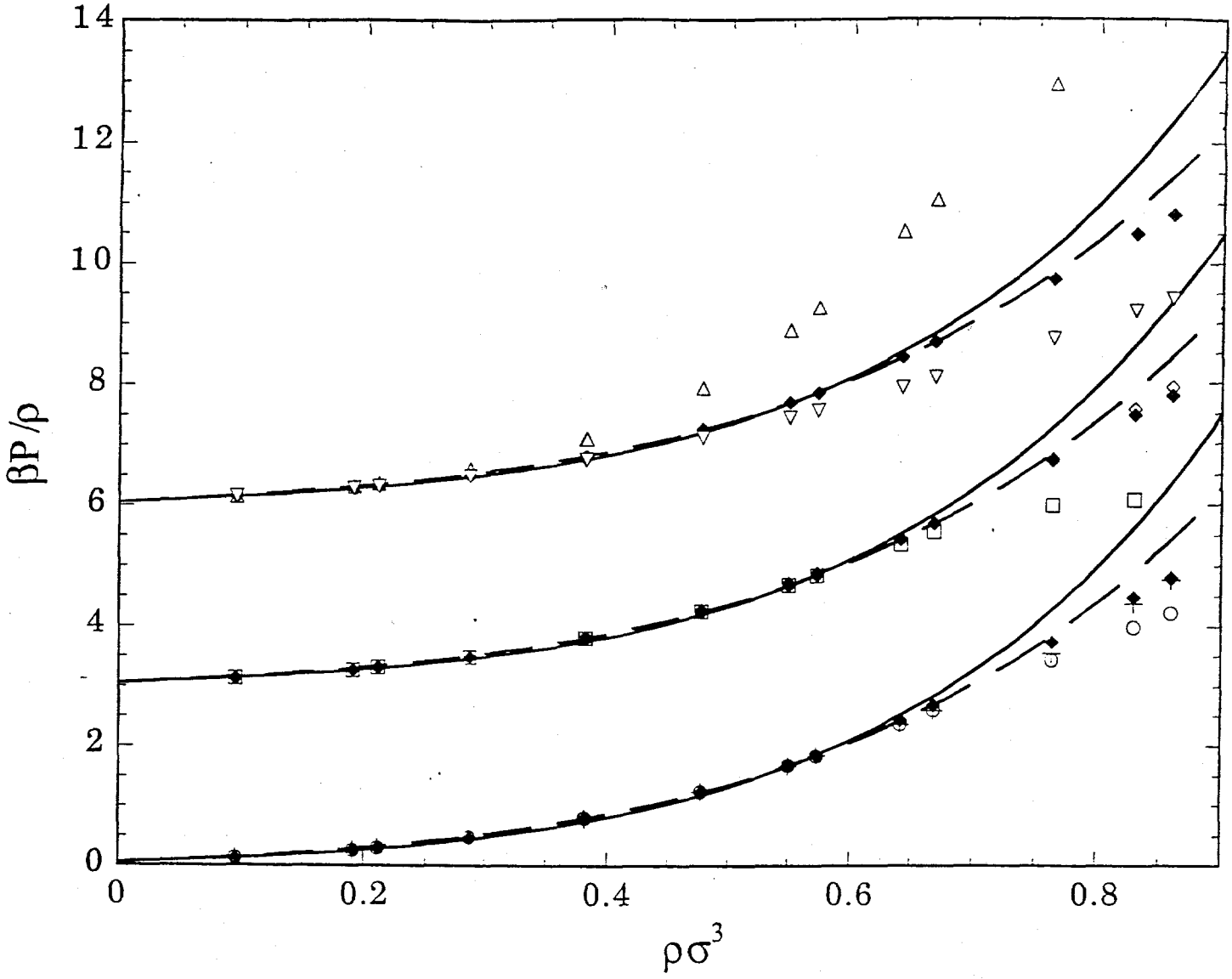


Figure 4

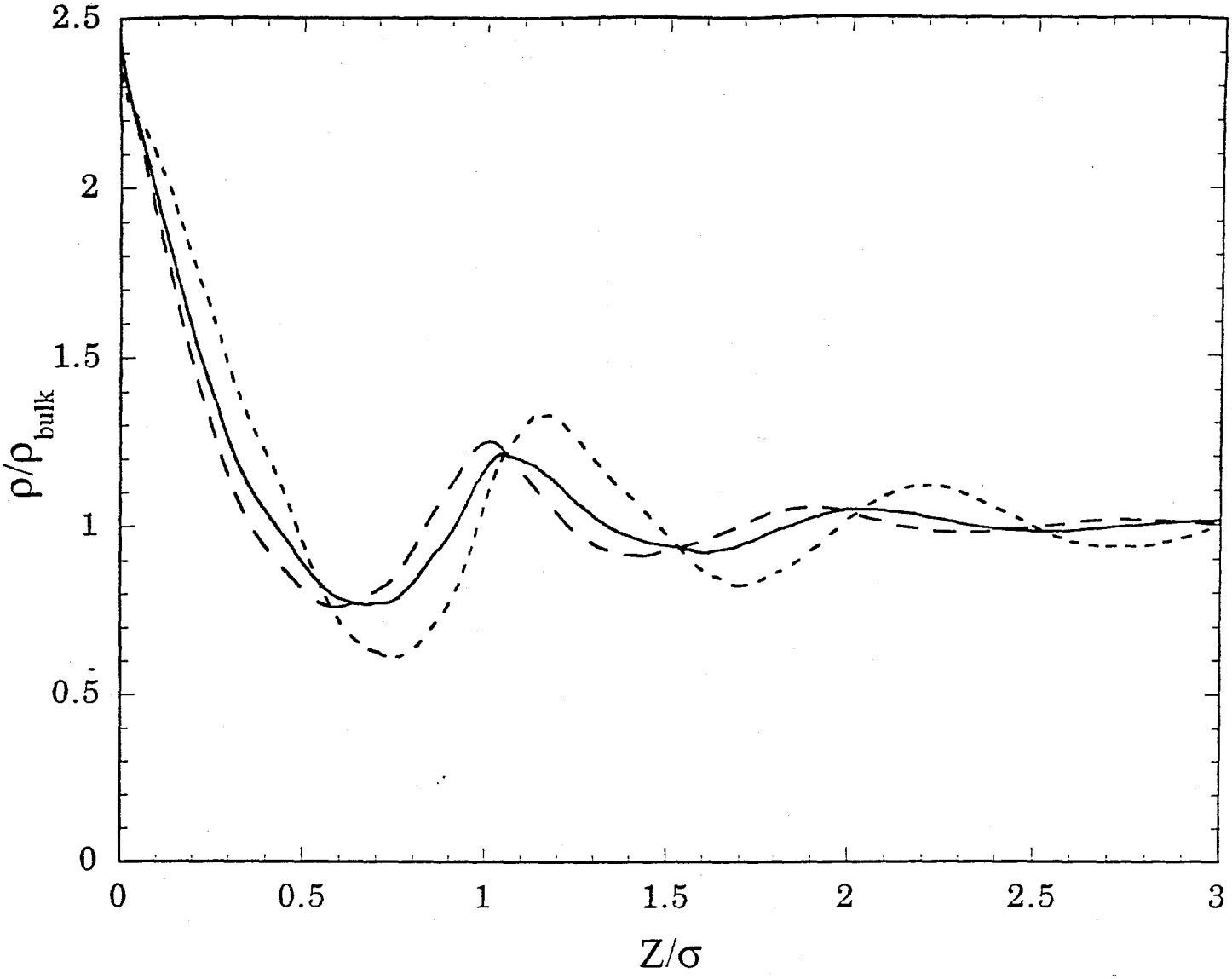


Figure 5

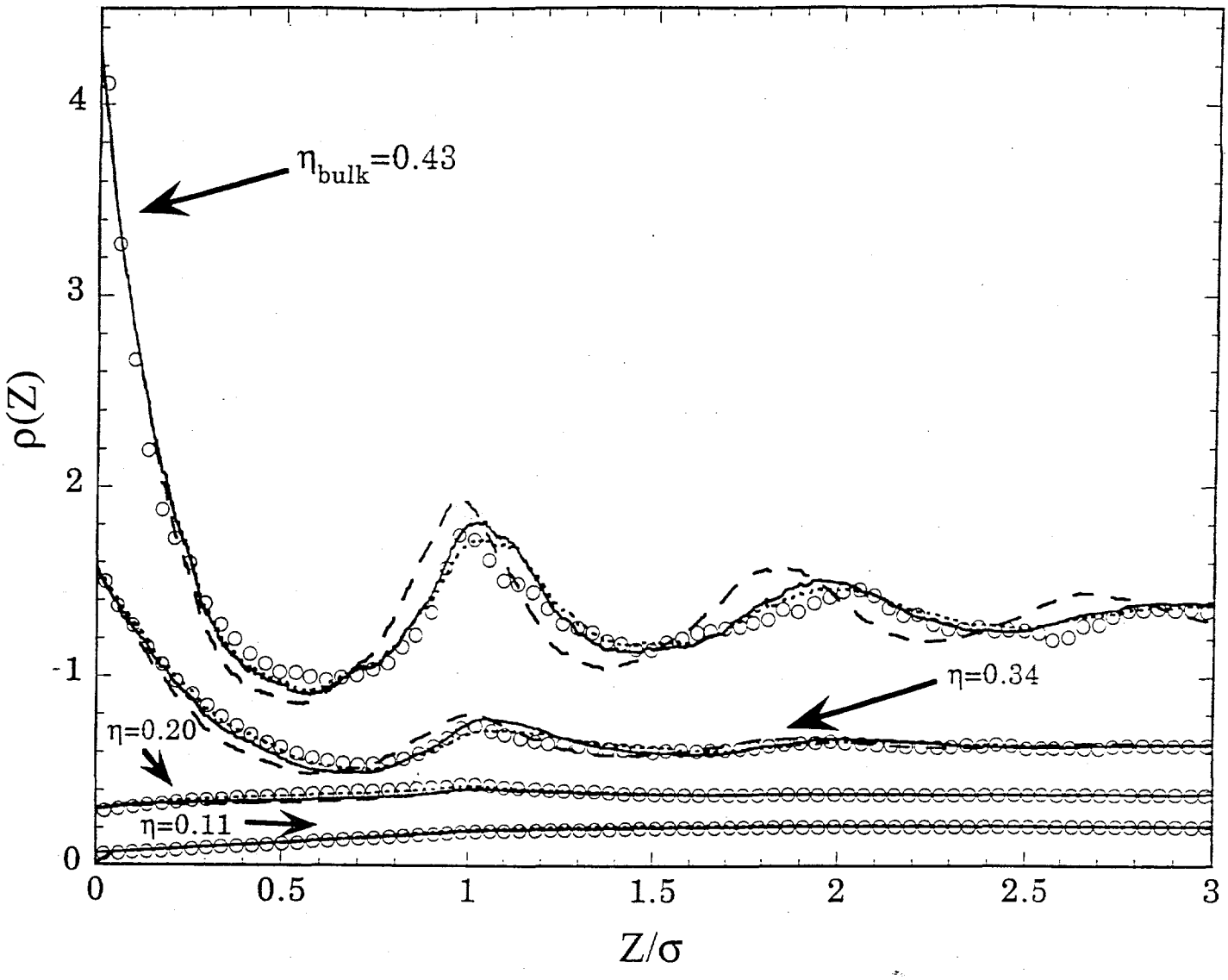


Figure 6

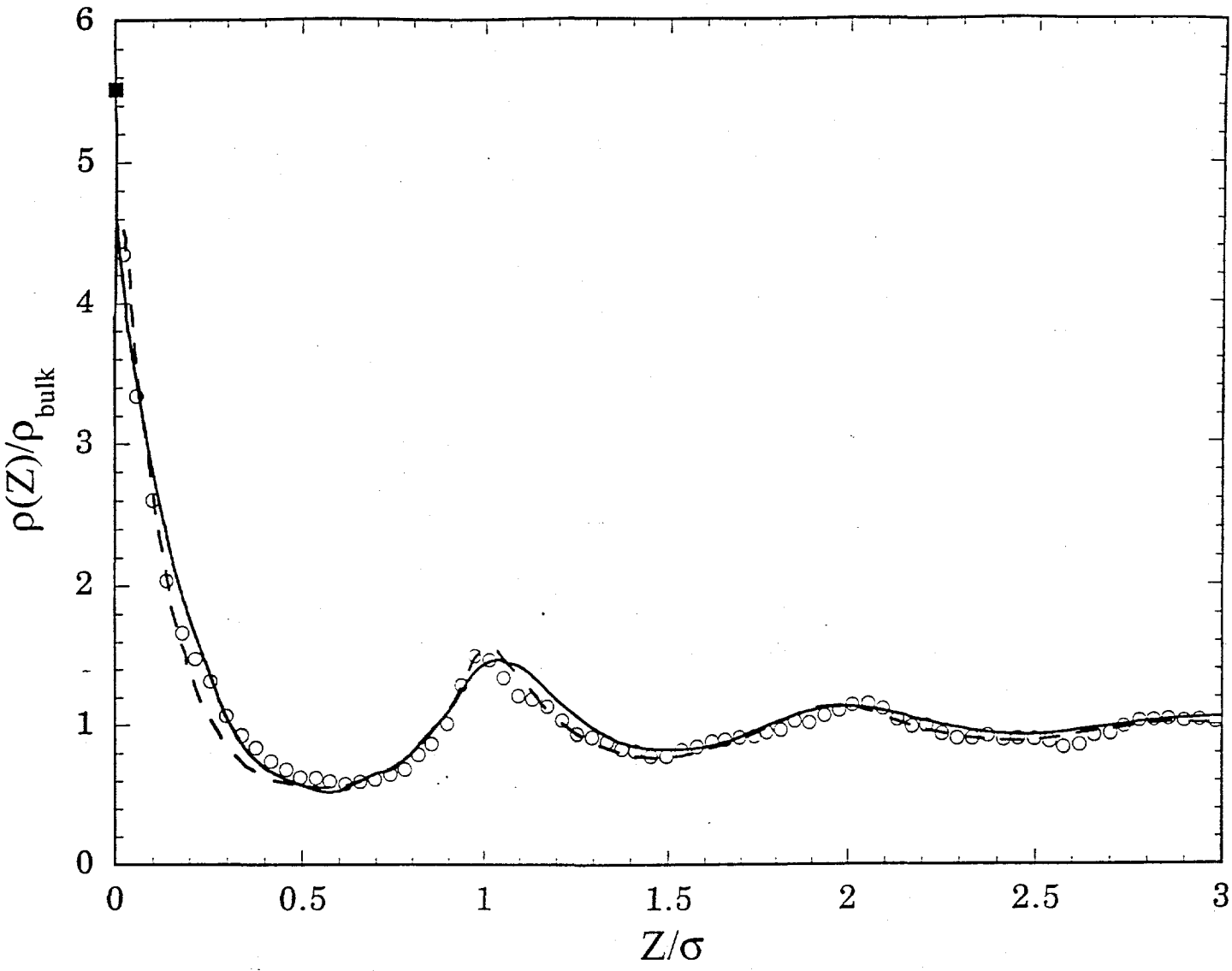


Figure 7

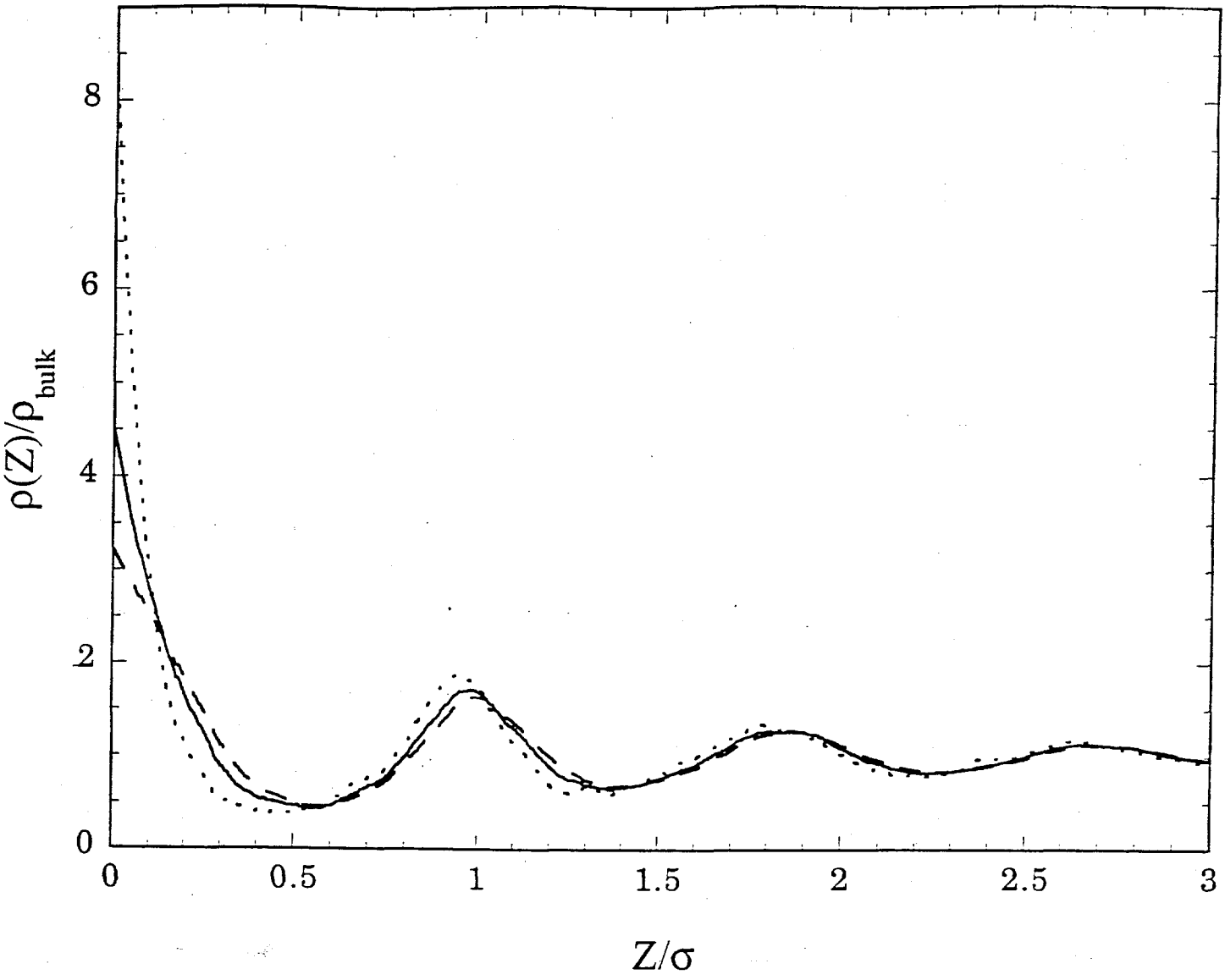


Figure 8

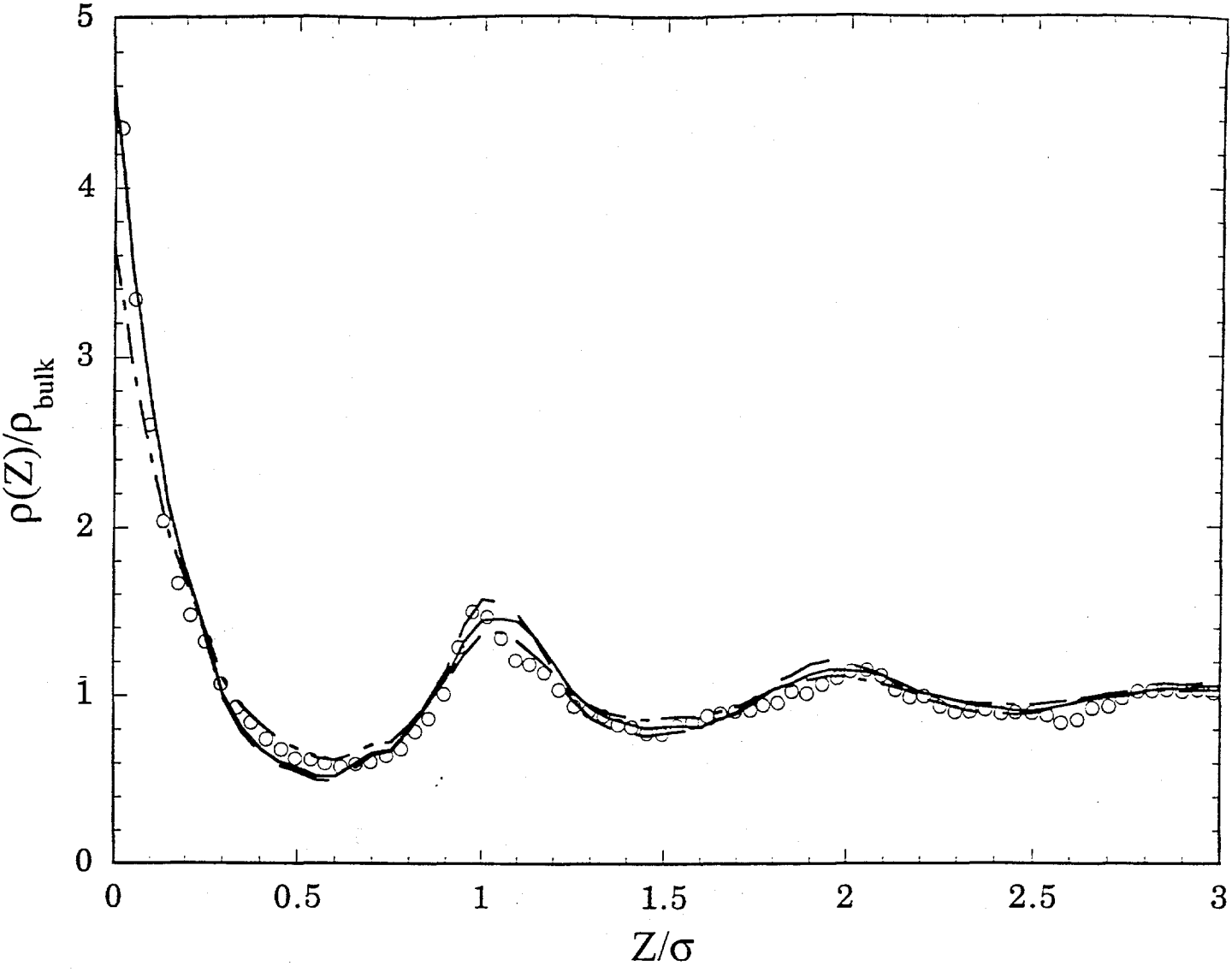


Figure 9

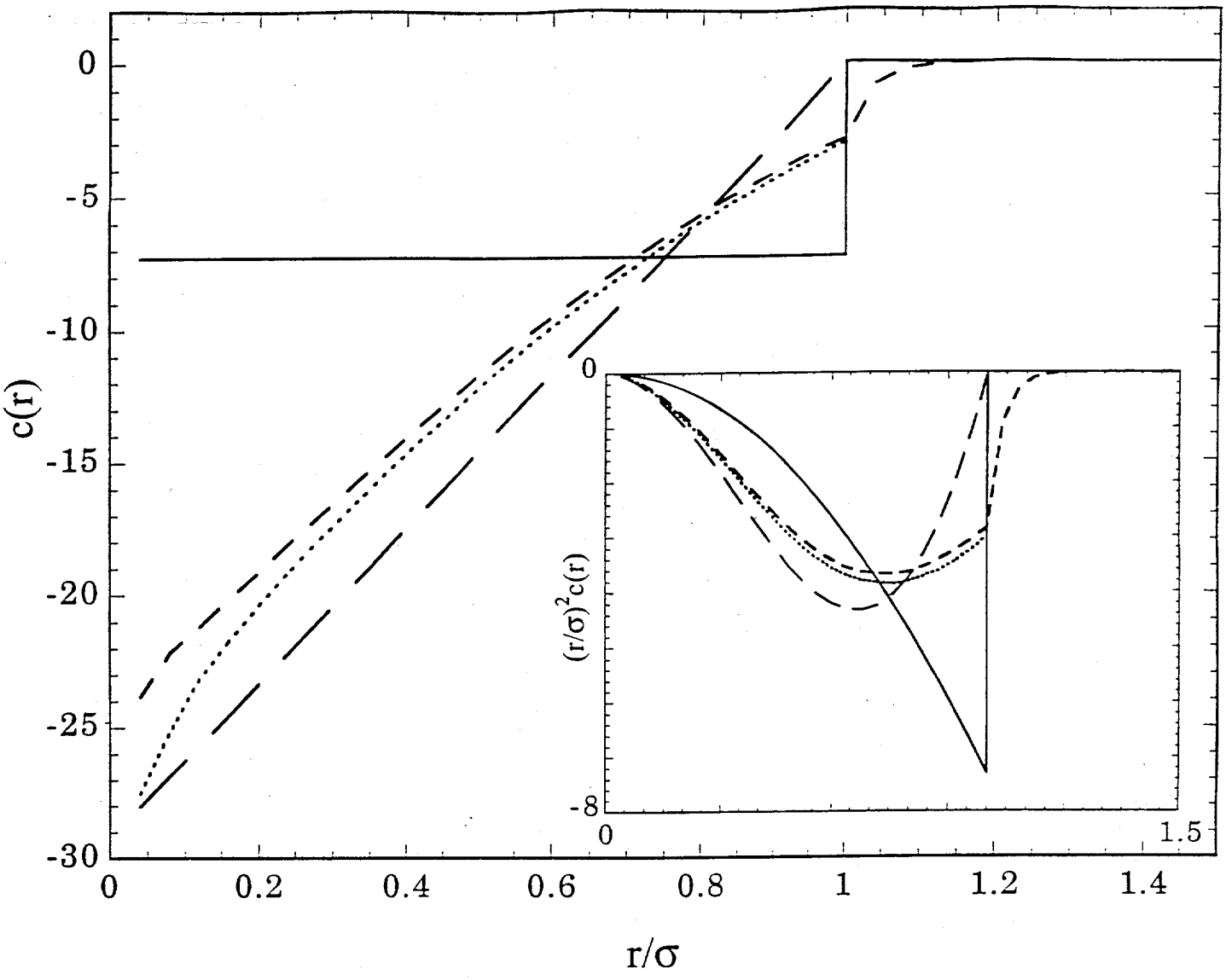


Figure 10

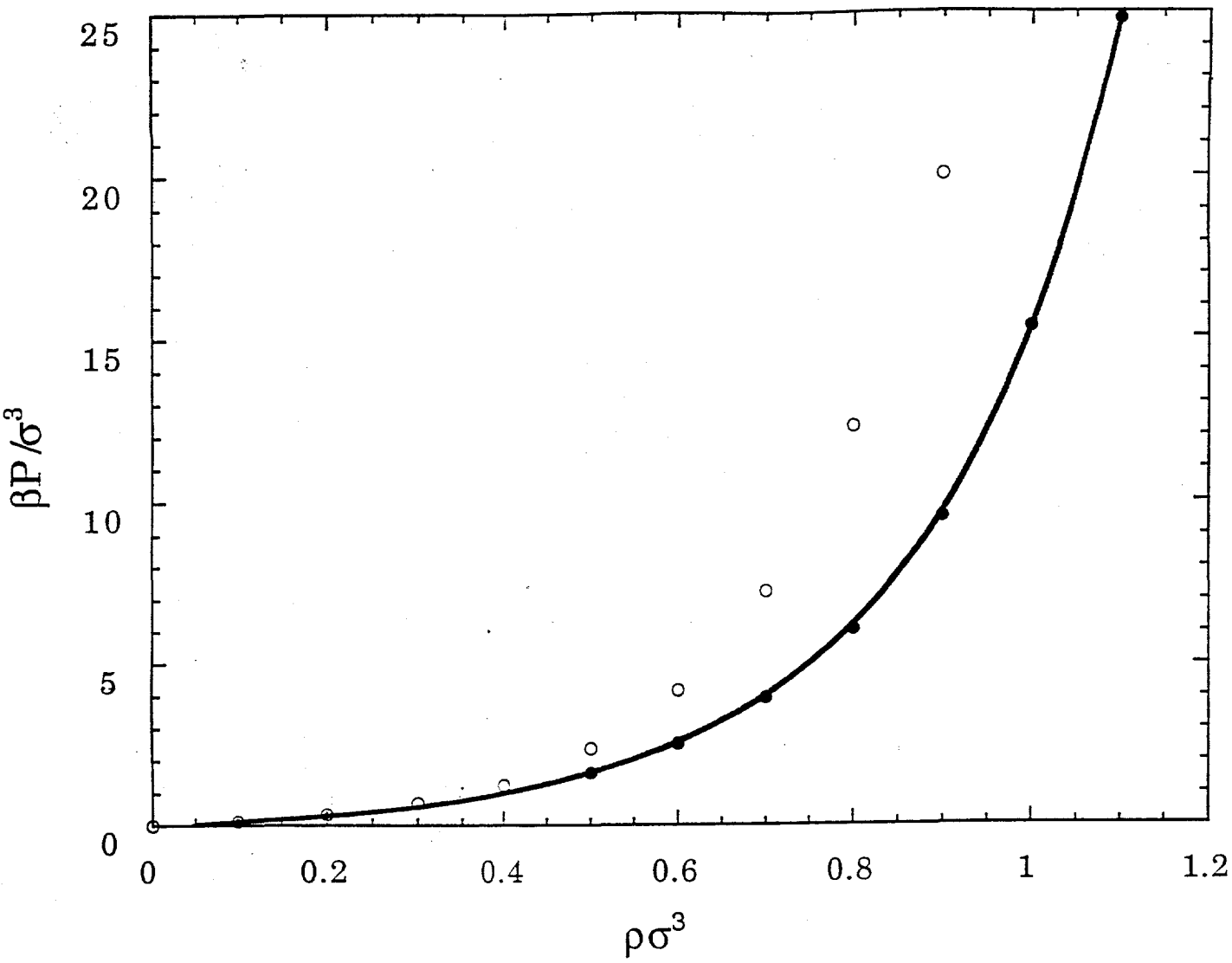


Figure A.1